Low Insertion-Loss, Sharp-Rejection and Compact Microstrip Low-Pass Filters

Mrinal Kanti Mandal, *Student Member, IEEE*, Priyanka Mondal, *Student Member, IEEE*, Subrata Sanyal, *Member, IEEE*, and Ajay Chakrabarty, *Senior Member, IEEE*

***Abstract*—Complementary split ring resonators are used to design compact, low insertion loss (IL), low pass filter with sharp cut-off. A prototype filter implementing area is 0.23 $\lambda_g \times 0.09\,\lambda_g$, λ_g being the guided wavelength at 3-dB cut-off frequency (f_c) 1.887 GHz. Maximum IL is within 0.5 dB up to 1.717 GHz and 20-dB stopband extends up to 3.4f_c.**

***Index Terms*—Complementary split ring resonators (CSRR), low pass filter (LPF), microstrip, stub.**

I. Introduction

IN MICROWAVE systems, low-pass filters (LPF) are often used to remove undesired harmonics or spurious mixing products. Stepped impedance LPF and open stub LPF are commonly used for this purpose. But, these filters have gradual cut-off response. By increasing the number of sections, the rejection characteristic can be improved. However, increasing the number of sections increases pass-band insertion loss (IL) and the physical size of the filter. Several techniques have been reported to address this problem. In [1], a LPF employing a semi-lumped element composed of a lumped capacitor and a section of transmission line was proposed. Multisection LPFs using microstrip line and interdigital capacitors [2], coupled lines [3] and stepped-impedance hairpin resonators [4] are the other approaches.

In this letter, an LPF unit section employing complementary split ring resonators (CSRRs) is proposed. A CSRR is the negative image of a split ring resonator (SRR) and produces a sharp rejection stop band [5] in the vicinity of its resonance frequency. In [6], CSRRs were used to design bandpass filtesr (BPFs). In [7], stopband responses of microwave filters were improved using multiple CSRRs. Here, CSRRs are proposed to design an LPF unit for the first time.

II. LPF Design

Fig. 2 shows the wideband simulated S-parameters of a CSRR loaded microstrip line with CSRR orientations $\theta = 0°$ and 90° (see Fig. 1). Full wave simulator IE3D has been used for simulations. Both of the orientations show non-periodic transmission dips. These dips correspond to CSRR resonances.

Manuscript received April 15, 2006; revised July 20, 2006.

The authors are with the Electronics and Electrical Communication Engineering Department, Indian Institute of Technology, Kharagpur 721302, India (e-mail: mkmandal@ieee.org; mandal.mrinal@gmail.com; pri.mondal@gmail.com; mri_mndl@yahoo.com).

Digital Object Identifier 10.1109/LMWC.2006.884777

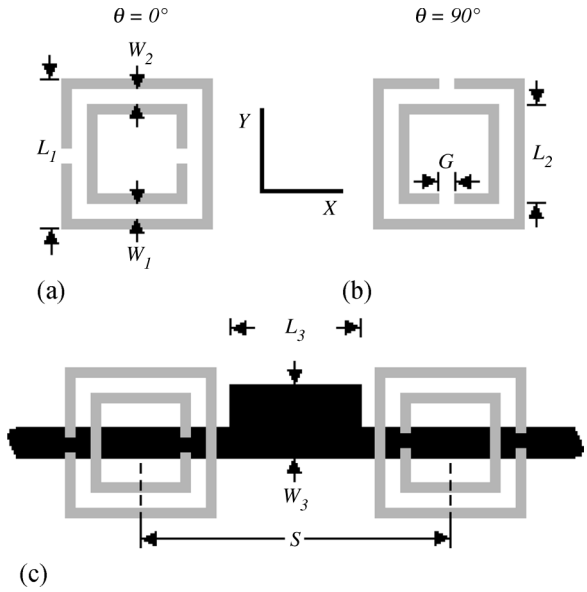

Fig. 1. CSRR in the ground plane with orientation (a) $\theta = 0°$, (b) $\theta = 90°$, and (c) configuration of the LPF, bottom view. Gray and black portion represents the etched CSRR and the microstrip part, respectively.

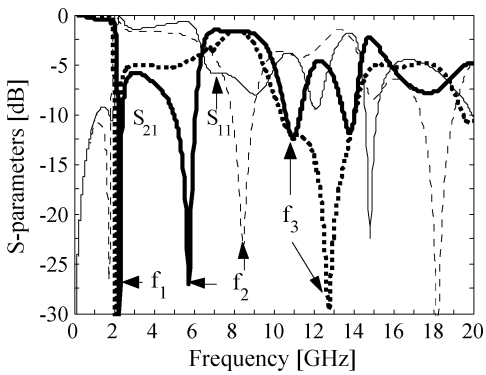

Fig. 2. Simulated S-parameters with $\theta = 0°$ (solid line) and 90° (dotted line). CSRR dimensions: $L_1 = 10.3$, $L_2 = 9.2$, $W_1 = 0.5$, $W_2 = 0.6$ and $G = 0.5$ mm. Substrate specifications: thickness = 0.381 mm and $\varepsilon_R = 2.2$.

For both of the orientations, at the first resonance frequency (f_1), the induced magnetic currents in each ring flows in the same direction, as shown in Fig. 3. The total current flowing on both of the rings remains the same for any cross section of the structure. Compared to it's dual structure SRR, this is quasistatic resonance [8]. At other dips, current distributions show that these are dynamic resonances. Here, a square shaped CSRR in place of a conventional circular shape is used for compactness.

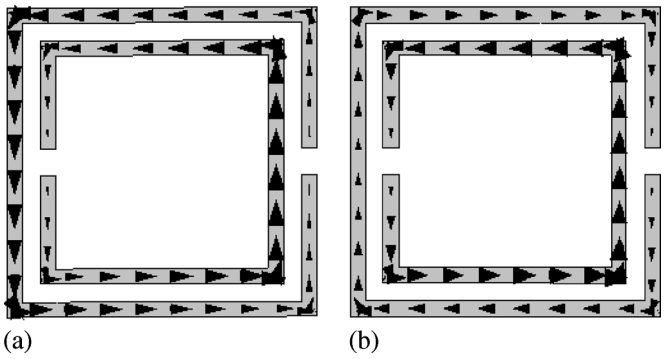

Fig. 3. Simulated induced magnetic current in the CSRRs for $\theta = 0^\circ$ orientation under (a) quasi-static and (b) dynamic condition.

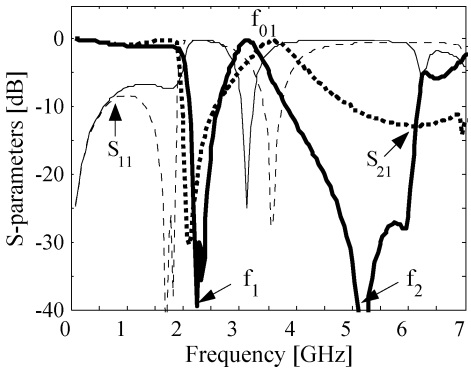

Fig. 4. Simulated S-parameters of coupled CSRRs with $\theta = 0^\circ$ (solid line) and 90° (dotted line). $S = 13.3$ mm and CSRR dimensions remain the same.

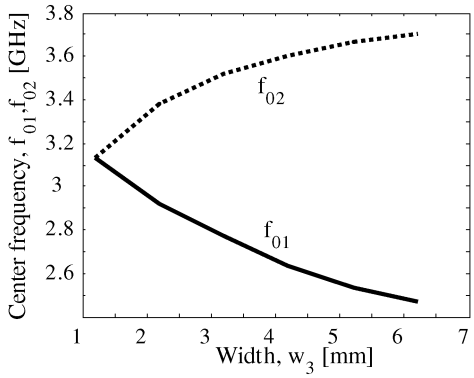

Fig. 5. Variation of passband center frequency with stub width for $\theta = 0^\circ$. For f_{01}: $L_3 = 2$ and $S = 13.3$ mm. For f_{02}: $L_3 = 15$ and $S = 37.7$ mm. CSRR dimensions remain the same.

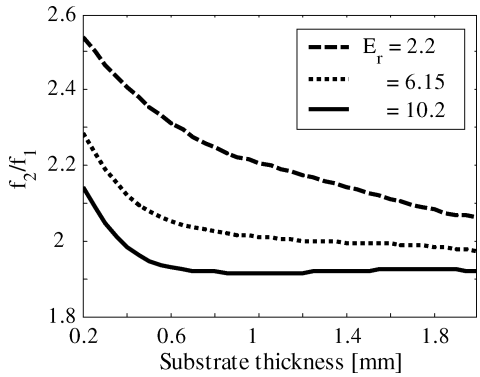

Fig. 6. Variation of the second resonance frequency (f_2) with substrate specifications $(\theta = 0^\circ)$.

The transmission responses (see Fig. 2) show that, IL in the passband below f_1 is lower, while it is considerably higher in the upper one (between first and second resonance frequencies f_1 and f_2, respectively). This loss is due to impedance mismatch between the CSRR loaded microstrip line and feed line. The second passband between f_1 and f_2 can be utilized as the stopband of the LPF by increasing its IL. To follow this idea, two CSRRs are cascaded and corresponding S-parameters are shown in Fig. 4. However, an undesired pass band appears at f_0, where center to center distance between the CSRRs (S) is $\lambda_g/4$; λ_g is the guided wavelength of CSRR loaded microstrip line at f_0. This passband is repeated for S equal to $n\lambda_g/4$, where, $n = 1, 3, 5\ldots$. This is because the $\lambda_g/4$ transmission line between the CSRRs acts as an admittance inverter with $J = 1$ and the passband appears due to impedance matching at f_0. The two orientations introduce different loading effect to the microstrip lines and hence there is a slight difference between the passband center frequencies. Let us call these pass band center frequencies for different n as f_{0n}. Increasing S decreases f_{0n}. At a certain S, f_{01} becomes smaller than f_1 and the pass band due to $n = 1$ disappears. But, at the same time, f_{02} decreases and appears as another undesired passband between f_1 and f_2. Therefore, the problem of undesirable passband remains. To remove this undesired passband, a capacitive loading is introduced between the CSRRs in the form of shunt open circuited stub. As shown in Fig. 1(c), a stub of length L_3 and width W_3 is attached to the $\lambda_g/4$ transmission line. Due to this capacitive loading, f_{01} shifts towards lower frequency while f_{02} towards higher frequency. Increasing capacitance decreases f_{01} but increases f_{02}, i.e., the mode separation increases. Fig. 5 shows the variation of f_{01} and f_{02} with stub-width W_3 for $\theta = 0^\circ$. Similar variation is observed for $\theta = 90^\circ$. Finally, at an optimized capacitance, f_{01} becomes lower than f_1, while f_{02} becomes higher than f_2 and a wide stopband is obtained from f_1 to f_2. It can be noted that, the second resonance frequency for $\theta = 90^\circ$ orientation is much higher than that for $\theta = 0^\circ$ orientation and a wider stopband may be realizable. But in this case, the required capacitance to diminish the undesired passband between f_1 and f_2 is so high that LPF pass band response degrades. Hence, $\theta = 0^\circ$ orientation is preferred for LPF design.

To design the LPF, in the first step, CSRR dimension is chosen in such a way that CSRR first resonance frequency (f_1) is equal to 3-dB cutoff frequency (f_c) of the LPF. The dimension can be approximately obtained using the formula given in [5]. Finally, it is optimized using IE3D. Center to center distance (S) between the CSRRs is taken equal to $\lambda_g/4$ at a frequency f_{01} which is slightly greater than f_c. Next, a shunt capacitive stub is introduced to make $f_{01} < f_1$ and $f_{02} > f_2$. Unless and until the capacitance is too high, CSRR resonance frequencies remain unaffected. The LPF rejection bandwidth depends on f_1 and f_2. Rejection bandwidth increases for higher f_2/f_1. As shown in Fig. 6, f_2 increases with decreasing dielectric constant and substrate thickness. Therefore, a substrate of lower dielectric constant and thickness is preferred for higher rejection band width.

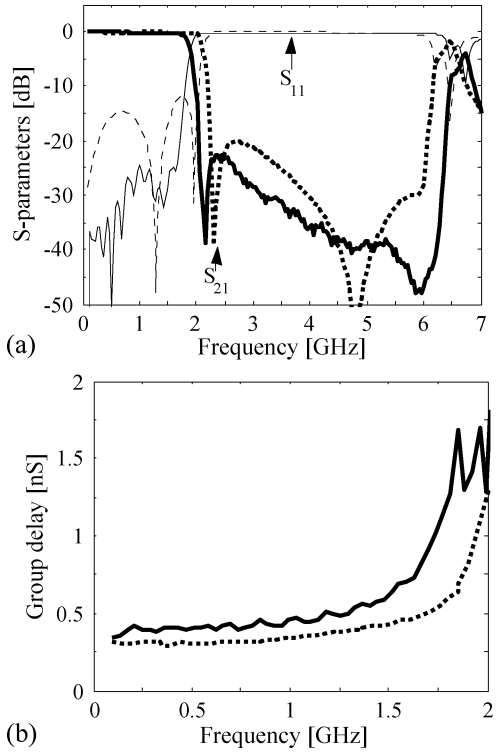

Fig. 7. Measured (solid line) and simulated (dotted line): (a) S-parameters and (b) group delay variation.

Rejection bandwidth can be further increased cascading another LPF having f_c nearly equal to f_2 of the first LPF. This procedure however increases implementation area. The connecting length between these two LPFs is adjusted for optimum passband response.

III. Fabrication and Measurements

A prototype LPF is fabricated on a 0.381 mm thick Rt/duroid 5880 substrate having dielectric constant $\varepsilon_R = 2.2$. LPF dimensions are: $L_1 = 10.3, L_2 = 9.2, L_3 = 5.6, W_1 = 0.5, W_2 = 0.6, W_3 = 5$, $G = 0.9$, and $S = 16$ mm. Simulated and measured responses of the filter are shown in Fig. 7. Measurements have been done using the HP8510C vector network analyzer. The measured 3-dB cutoff frequency (f_c) of the filter is 1.887 GHz. Maximum passband IL is within 0.35 dB up to 1.66 GHz. The filter has a sharp passband to stopband transition knee. The maximum attenuation rate is 130 dB/GHz (attenuation being 3 and 38.5 dB at 1.887 and 2.146 GHz, respectively). Sharp rejection property of CSRR enables to achieve such a high selectivity using only two resonators. Maximum group delay variation in the passband [see Fig. 7(b)] is within 1.4 nS. A 20-dB stopband extends up to $3.4 f_c$.

IV. Conclusion

This paper presents a new technique to design a high performance LPF unit section using CSRR. The filter has the advantages of sharp cutoff, compactness, and low passband IL. Due to sub-lambda dimensions of CSRRs, the filter occupying area is $0.227\,\lambda_g \times 0.089\,\lambda_g$. In addition, the proposed filter has low passband IL. It is easy to fabricate as no lumped elements or via holes are used. A single section CSRR LPF is superior to that of [1]–[4] in terms of rejection rate at transition knee and passband IL, and in terms of compactness [2]–[4].

References

[1] J.-W. Sheen, "A compact semi-lumped low-pass filter for harmonics and spurious suppression," *IEEE Microw. Wireless Compon Lett.*, vol. 10, no. 3, pp. 92–93, Mar. 2000.

[2] W.-H. Tu and K. Chang, "Compact microstrip low-pass filter with sharp rejection," *IEEE Microw. Wireless Compon. Lett.*, vol. 15, no. 6, pp. 404–406, Jun. 2005.

[3] Y.-W. Lee, S.-M. Cho, G.-Y. Kim, J.-S. Park, D. Ahn, and J.-B. Lim, "A design of the harmonic rejection coupled line low-pass filter with attenuation poles," in *IEEE MTT-S Int. Dig.*, 1999, pp. 682–685.

[4] L.-H. Hsieh and K. Chang, "Compact elliptic-function low-pass filters using microstrip stepped-impedance hairpin resonators," *IEEE Trans. Microw. Theory Tech.*, vol. 51, no. 1, pp. 193–199, Jan. 2003.

[5] J. D. Baena, J. Bonache, F. Martin, R. M. Sillero, F. Falcone, T. Lopetegi, M. A. G. Laso, J. Garcia-Garcia, I. Gil, M. F. Portillo, and M. Sarolla, "Equivalent-circuit models for split-ring resonators and complementary split-ring resonators coupled to planar transmission lines," *IEEE Trans. Microw. Theory Tech.*, vol. 53, no. 4, pp. 1451–1461, Apr. 2005.

[6] J. Bonache, I. Gil, J. Garcia-Garcia, and F. Martin, "Novel microstrip bandpass filters based on complementary split-ring resonators," *IEEE Trans. Microw. Theory Tech.*, vol. 54, no. 1, pp. 265–271, Jan. 2006.

[7] J. Garcia-Garcia, F. Martin, F. Falcone, J. Bonache, J. D. Baena, I. Gil, E. Amat, T. Lopetegi, A. G. Laso, J. A. M. Iturmendi, M. Sorolla, and R. Marques, "Microwave filters with improved stopband based on sub-wavelength resonators," *IEEE Trans. Microw. Theory Tech.*, vol. 53, no. 6, pp. 1997–2006, Jun. 2005.

[8] J. Garcia-Garcia, F. Martin, F. Falcone, J. Bonache, I. Gil, T. Lopetegi, M. A. G. Laso, M. Sorolla, and R. Marques, "Spurious passband suppression in microstrip coupled line band pass filters by means of split ring resonators," *IEEE Microw. Wireless Compon. Lett.*, vol. 14, no. 9, pp. 416–418, Sep. 2004.